

Title: Evidence for an additional planet in the β Pictoris system

Authors: A.-M. Lagrange^{1(*)}, Nadège Meunier¹, Pascal Rubini², Miriam Keppler^{1,3}, Franck Galland¹, Eric Chapellier⁴, Eric Michel⁵, Luis Balona⁶, Hervé Beust¹, Tristan Guillot⁴, Antoine Grandjean¹, Simon Borgniet¹, Djamel Mekarnia⁴, Paul Anthony Wilson^{7,8,9}, Flavien Kiefer⁷, Mickael Bonnefoy¹, Jorge Lillo-Box¹⁰, Blake Pantoja^{10,11}, Matias Jones¹⁰, Daniela Paz Iglesias^{12,13}, Laetitia Rodet¹, Matias Diaz¹⁴, Abner Zapata¹⁵, Lyu Abe⁴, François-Xavier Schmider⁴

Affiliations:

¹ Institut de Planétologie et d'Astrophysique de Grenoble, Univ Grenoble Alpes, CNRS, IPAG, 38000 Grenoble, France

² Pixyl, 5 Avenue du Grand Sablon, 38700 La Tronche, France

³ Max Planck Institute for Astronomy, Königstuhl 17, 69117, Heidelberg, Germany

⁴ Université Côte d'Azur, OCA, Lagrange CNRS, 06304 Nice, France

⁵ PSL, LESIA, CNRS, Sorbonne Université, Université Paris Diderot, Observatoire de Paris, 92195, Meudon Cedex, France

⁶ South African Astronomical Observatory, P.O. Box 9, Observatory, Cape 2735, South Africa

⁷ CNRS, UMR7095, Institut d'Astrophysique de Paris, 98bis Boulevard Arago, 75014, Paris, France

⁸ Department of Physics, University of Warwick, Coventry CV4 7AL, UK

⁹ Leiden Observatory, Leiden University, Postbus 9513, 2300 RA Leiden, The Netherlands

¹⁰ European Southern Observatory, Alonso de Córdova 3107 Vitacura, Santiago, Chile

¹¹ Departamento de Astronomía, Universidad de Chile, Camino el Observatorio 1515, Las Condes, Santiago, Casilla 36-D, Chile

¹² Instituto de Física y Astronomía, Facultad de Ciencias, Universidad de Valparaíso, Av. Gran Bretaña 1111, 5030 Casilla, Valparaíso, Chile

¹³ Núcleo Milenio de Formación Planetaria - NPF, Universidad de Valparaíso, Av. Gran Bretaña 1111, Valparaíso, Chile

Summary

With its imaged debris disk of dust, its evaporating exocomets, and an imaged giant planet, the young (~ 23 Myr) β Pictoris system is a unique proxy for detailed studies of planet formation processes as well as planet-disk interactions. Here, we study 10 years of ESO/High Accuracy Radial velocity Planet Searcher (HARPS) high resolution spectroscopic data of β Pictoris. After removing the radial velocity signals arising from the δ Scuti pulsations of the star, a ~ 1200 days periodic signal remains that, within our current knowledge, we can only attribute to a second planet in the system. β Pictoris c mass is ~ 9 times the mass of Jupiter; it orbits at ~ 2.7 au on an eccentric ($e \sim 0.24$) orbit. More RV data are needed to get more precise estimates of β Pictoris c properties. The current modelling of the planets properties and the dynamic of the whole system has to be reinvestigated in the light of this detection.

After 25 years, our view of the planetary systems architectures has profoundly evolved thanks to the detection of a large variety of exoplanets. In particular, giant planets which orbit between a few stellar radii (detected by means of indirect techniques such as radial velocity variations or transit) up to several hundreds of au (detected by direct imaging) from their stars have been found. This diversity suggests different ways in which giant planets or low mass brown dwarfs may form; it also suggests that after formation, dynamical evolution (disk migration, third body interaction) plays a significant role in determining the final architecture of the planetary systems ¹.

Young systems aged between ~ 5 and 50 Myr offer a particularly interesting opportunity to study the early stages of planet formation and evolution, when giant planets are formed and most of the protoplanetary gas has been removed from the disk. The

~23 Myr β Pictoris system is an emblematic prototype of such systems. Its resolved debris disk of dust ² is attributed to collisions among planetesimals orbiting between ~50 and 100 au ^{3,4}. Evaporating exocomets ⁵ were detected and a giant planet ^{6,7}, β Pic b, has been imaged orbiting at about 9 au from the star. Gravitational interaction between β Pic b and the planetesimals, together with stellar radiation pressure can explain most of the disk morphological properties, especially the prominent inner warp ^{8,3,9}, and the dust outward extension. β Pic b could be responsible for triggering the infall and evaporation of the exocomets on to the star (so-called Falling Evaporating Bodies -FEB- scenario¹⁰).

Thermal data ^{11,12,13} revealed gaps and knots that suggest additional planets at separations larger than 20 au. The apparent void of material within about 50 au from the star suggests that planets might be present in this region ¹⁴. In addition, Atacama Large Millimeter Array (ALMA) observations revealed side asymmetries that could be due to the presence of other planets in the system ⁴. Finally, the slightly inclined orbit of β Pic b could be due to the gravitational perturbation by another, yet unseen planet.

Recently, HARPS high precision spectroscopic data were combined with the Very Large Telescope Nasmyth adaptive optics and Conica system (NaCo) high spatial resolution imaging data to search for additional giant planets on a wide range of separations from 0.01 to 100+ au from the star ¹⁵, bridging for the first time the gap between radial velocity (RV) and direct imaging detection limits in the planetary/brown dwarf domain. It turns out that companions with masses $4 M_{Jup}$ or more orbiting closer than 1 au or further than 10 au are not present in the system. The 2-6 au region is somewhat less constrained, with limits in the $10 M_{Jup}$ to brown dwarf masses range. Adding more recent extreme-AO SPHERE data improves the detection limit and allows excluding companion planets more massive than about $15 M_{Jup}$, and with separations 2-6 au.

The data

We analysed 6645 HARPS high resolution ($R=120000$), high signal-to-noise (SN, mean SN of 273 at 550 nm) spectra of β Pictoris obtained between 2003 and 2018. Observations prior to 2008 consist of exposures of a few minutes designed to study the variability of Ca II absorption lines attributed to the exocomets mentioned above. After the discovery of β Pictoris b, the monitoring of the star was intensified to constrain the mass of the planet through radial velocity measurements^{16,17}. However, high frequency stellar pulsations with amplitudes up to 1200 m/s, dominate the RV variations and represent a major source of noise. Pulsations modes at 47.44, 38.06 and 47.28 cycle.d⁻¹ have been reported¹⁸ using photometric data. These pulsations were also seen in the line profiles analysis of about 700 spectra obtained over two weeks¹⁹. They indicate that the star is a member of the δ Scuti group. Recently, high quality data acquired from the Concordia research station in Antarctica during a long-term monitoring of β Pictoris between April and October 2017 allowed the identification of 31 sinusoidal pulsations²⁰. To mitigate the impact of the stellar pulsations on the RV analysis, we adopted after 2008 a specific observing strategy that consisted in monitoring the stellar variations on uninterrupted sequences of 1-2 hours and correcting for them. Furthermore, a few longer (~6h) sequences were obtained in 2017-2018. After appropriate data selection (see Methods), the RVs measured after 2008 are plotted in Fig. 1a together with an example of the pulsation pattern (Fig. 1b). We note that the uncertainties associated to the RV are higher than in the case of Main Sequence solar-type stars, because β Pic is an early type star (A5V), with fewer spectral lines, and a much higher rotational velocity (120 km/s) than Main Sequence solar-type stars, which have rotational velocities in the range 3-5 km/s.

The periodogram of the RV data (Fig. 1c) reveals a complex set of peaks, most of them well above the 10% False Alarm Probability level. These peaks are not due to noise but for most of them to a combination of pulsation modes and of the complex temporal distribution of our data. The highest peak of the periodogram is at \sim 1200 days. It is not associated to β Pic b's orbital period (\sim 7800 days). We show in Fig. 1d the periodogram for the temporal window by replacing our RV data by a linear function of the Julian date. Over the entire range of periods, peaks are present but not at 1200 d. This shows that while a large fraction of the peaks in Fig. 1c are due to the uneven temporal distribution of the observations, this is not the case of the 1200 d peak.

To further study the signal associated with this \sim 1200 d peak, the data must be corrected first from the complex, high-frequency pulsation patterns. To do so, different methods described in Methods were used. The first, straightforward approach was to average the RV obtained from continuous sequences of data obtained over 1-2 hr or more. To perform such analysis, only the well sampled and long enough data sequences obtained after 2008 were retained. More sophisticated approaches consisted in fitting each of the longest sets of data, once grouped in bins of less than 8 days, with sine series describing the RV variations due to the pulsations, plus an offset either in an iterative way, or simultaneously. The time series of the residuals obtained after subtracting the sine functions and the time series of the offsets can then be analysed.

Altogether, the sine fits confirm the presence of multiple pulsations with frequencies in the range 35-65 cycles.d⁻¹ as detected in photometry, but also, possibly, weaker pulsations in the 3-4 cycles.d⁻¹ range, characteristic of γ Dor pulsations (see Methods for more details).

The residual RVs obtained after subtracting the pulsations-induced RV variations are shown in Figure 2. Their periodogram shows again a prominent peak at \sim 1200 d. The offsets also exhibit long-term variations with a total amplitude of about 200 m/s (Fig. 2), and their periodogram shows again the same peak.

Possible origins of the remaining RV signal and of the observed \sim 1200-d peak

We first ruled out systematic observing errors due to temporal variations in air mass, proximity of the Moon or variations in the S/N level because they show no correlation with the corrected RV residuals.

Instrumental systematic effects can also be ruled out because the observed amplitude of over 300 m/s would have been detected on other stars observed with the same set-up. Amplitudes as low as 1–10 m/s have been obtained for the RV variation of low-mass planets around solar type stars. Instrumental effects that would only affect rapid rotators would have been detected in our previous surveys of A-F stars.

An artifact due to the temporal sampling was searched for. The probability of a fortuitous origin of the 1200-d period was estimated to be less than 10^{-3} (see Methods).

Stellar pulsations with periods 1–100 d, which are not well sampled with the present data cannot explain the \sim 1200 d peak. We checked that such pulsations would not create a high peak at 1200 d. Periods of the order of 1200-d of stellar origin have not been reported for stars similar to β Pictoris (and would be extremely difficult to measure). We note that radial pulsations that would produce RV variations with amplitudes of more than 100 m/s and a period of 1200 d can definitely be excluded as they would indicate a radius variation of several hundreds of stellar radii, which is not possible.

The possibility of an artifact due to an incomplete removal of the stellar pulsations was investigated in depth (see Methods). Within the current knowledge on hybrid δ Scuti and γ Dor stars, a stellar origin is not possible.

No correlation between the offsets and the presence of exocomets absorptions is found. Examples of such events are given in Supplementary Figure 3 of the Methods, together with the computed offsets at the same epochs.

We therefore conclude that, under our today knowledge, these long-term radial-velocity variations must be caused by an additional companion.

An additional planet

Hereafter, we assume that the RV residuals are due to the combination of β Pictoris b and of the additional companion. The pulsation-subtracted RV data series, as well as the offset series, were fitted with two Keplerian functions, accounting respectively for β Pictoris b and for the additional companion, plus an offset (hereafter referred to as the global offset) to account for the fact that the RV are computed relative to a reference spectrum (see Methods). An evolutionary algorithm similar to the one used to fit the pulsations was used. A mass of $1.75 M_{\odot}$ was assumed for the star²¹.

β Pictoris b known orbital properties and associated uncertainties have to be taken into account. The astrometric orbit of β Pictoris b was fitted independently using our MCMC software applied to high contrast images²². This resulted in a collection of 500,000 orbits that represents the posterior distribution of β Pictoris b's orbital elements. We selected a subset of 219 orbits out of this sample with the following criteria: semi-major axis $a=9.0+/-0.4$ au (1 sigma in the main peak), eccentricity $e<0.055$ and $\chi^2<19.2$. These criteria ensure that the best possible solutions have been selected. For each of these solutions, we fitted the RV data. The free parameters for each fit were β Pic b mass, the additional companion mass and orbital parameters,

and a global offset. The mass of β Pic b was allowed to vary between 5 and $15 M_{\text{Jup}}$, a range which largely encompasses all published estimated masses, derived primarily from model-dependent brightness-mass relations. For the additional companion, an inclination of 90 degrees was assumed, which is reasonable as the system is seen nearly edge-on and β Pictoris b is only very slightly inclined (< 1 degree) with respect to the star equatorial plane. We then obtained 219 orbital solutions for the companion, as well as 219 masses for both β Pictoris b and the companion. An example of the 2-planet fit of the pulsations-corrected RV data is shown in Figure 3. This example corresponds to one of the very best solutions found among the 219 nominal ones; this solution is referred to as #108.

The distributions of the orbital parameters of the additional companion, of its mass, and of the mass of β Pictoris b are presented in Figure 4. The additional companion's semi-major axis is about 2.7 au, corresponding to a ~ 1220 d period. Its eccentricity is slightly greater than 0.2, and its mass, $8.9 M_{\text{Jup}}$, falls well in the planet range. It will be referred to as β Pictoris c in the following. The mass of β Pictoris b is found to be about $9.9 M_{\text{Jup}}$. Given that our total baseline is still shorter than the β Pictoris b period (see Fig.3), this mass is only indicative. We note it is compatible with recent estimates based on measured Hipparcos and GAIA astrometric measurements^{23,24}. We also note that the presence of β Pictoris c will itself require a re-examination of these astrometric constraints on the mass of β Pictoris b. Finally, we checked that a slightly different mass of β Pictoris b would not significantly change the mass of β Pictoris c. A similar conclusion is reached in case of a slightly different (a few %) mass for the star.

We conclude that the current data and knowledge on the star's properties provide very strong evidence of a giant planet in the system in the inner system, in addition

to β Pic b. Additional Harps data will be precious to strengthen this result and improve the planet characterisation. In the following, we discuss the impact of this result.

To our knowledge, β Pictoris is today the only system around which a planet is detected by direct imaging and a second planet is found by indirect techniques. β Pic is the second known multiple planetary system with at least one imaged planet. The first one is HR 8799, with four imaged planets of roughly equal masses and distances from 14 to more than 60 au^{25,26}. The planetary formation mechanism in HR 8799 is still unknown. Given their large orbits, HR 8799 b and c are good candidates for formation by gravitational instability in a disk. Given their small distance to their parent star, β Pic b and c are good candidates for in-situ formation by core accretion. Furthermore, we note that β Pic c orbits near the lower limit of the snow line position for a $1.75 M_{\odot}$ star²⁷.

The presence of a planet like β Pic c raises several dynamical issues for the system as a whole:

- The first is whether the two planets are dynamically stable. A quick analysis shows that indeed, the system is stable over a time of the order of its age (see Methods).
- A second issue concerns the relationship between β Pic c and the FEBs claimed to be responsible for strong, transient absorptions in the lines of ionized elements, monitored for years in β Pic spectrum since the eighties² (and references there-in). Even though no direct correlation is found between the exocomets absorptions (see Supplementary Figure 3 for examples of such absorptions) and the RVs variations, a possible link cannot be excluded (see Methods).
- Finally, it was proposed that β Pic b could be responsible for the debris disk inner warp if it is in a slightly inclined orbit⁴. Later, it was shown that the planet orbit was

indeed inclined ²⁸. The presence of β Pic c does not change significantly the conclusions, owing to its smaller distance from the star than β Pic b.

Future observations

The expected astrometric wobble produced by β Pic c is about 700 μ as, significantly smaller than the astrometric excess noise, 2.12 mas reported in the current GAIA Data Release, but it will be easily detected when all data become available (~2022). An aggressive monitoring of the β Pic RV variations will allow further constraining the planet orbital properties within the next two or three years.

A direct detection in imaging of β Pic c would allow a unique calibration to the brightness-mass relations for young stars. Such a calibration is required to accurately estimate the masses of directly imaged planets. It would also allow for a test of the planet formation mechanisms and, in particular, the way the material is accreted onto the planet embryo. Indeed, hot-start models of 9-10 M_{Jup} planets predict an H magnitude (at 21 Myr) more than 100 times higher than cold-start models ²⁹. The expected contrast between star and planet in H is about 10 magnitudes, assuming a hot-start model. The maximum projected separation depends on the detailed planet orbital properties but is in the range 0.1" - 0.15". Achieving such a contrast may be then possible with SPHERE, when the planet is at its maximum elongation. Note that given the present uncertainties on the orbital parameters, it is not possible to provide a precise date for this event. A contrast hundred times larger, on the contrary, would not be achievable with current instruments. Hence, a positive detection would favour a hot-start model and would provide a confirmation of the brightness prediction. A negative detection would be less conclusive, as it would mean that either the hot-start model predictions are overestimated or that the planet formed under a cold-start model.

Finally, because its semi-major axis is significantly smaller than that of β Pictoris b, β Pictoris c may transit its star. A transit of β Pic c would allow its atmosphere to be explored, while a transit of its Hill sphere would allow for the search for moons or circumplanetary rings. Co-orbital bodies trapped in the Lagrangian regions of β Pic c might also be searched for as they are common outcomes of planet formation hydrodynamical simulations.

References

1. Baruteau, C., Bai, X., Mordasini, C., Mollière, P. Formation, Orbital and Internal Evolutions of Young Planetary Systems *Space Science Reviews* 205, 77–124 (2016).
2. Smith, B. A., & Terrile, R. J., A circumstellar disk around β Pictoris, *Science* 226, 1421-1424 (1984).
3. Augereau, J. C., Nelson, R. P., Lagrange, A.-M., Papaloizou, J. C. B., & Mouillet, D., Dynamical modeling of large-scale asymmetries in the β Pictoris dust disk, *Astron. Astrophys.* 370, 447-455 (2001).
4. Dent, W., *et al.*, Molecular Gas Clumps from the Destruction of Icy Bodies in the β Pictoris Debris Disk, *Science* 383, 1490-1492 (2014).
5. Kiefer, F., *et al.*, Two families of exocomets in the β Pictoris system, *Nature* 514, 462 -464 (2014).
6. Lagrange, A.-M., A probable giant planet imaged in the β Pictoris disk. VLT/NaCo deep L'-band imaging, *Astron. Astrophys.* 493, L21-L25 (2009).
7. Lagrange, A.-M., *et al.*, A Giant Planet Imaged in the Disk of the Young Star β Pictoris, *Science*, 328, 57-59 (2010).

8. Mouillet, D., Larwood, J.D., Papaloizou, J. C. B., & Lagrange, A.-M., A planet on an inclined orbit as an explanation of the warp in the β Pictoris disc, *Mon. Not. R. Astron. Soc.* 292, 896-904 (1997).
9. Nesvold, E., & Kuchner, M. J., A SMACK Model of Colliding Planetesimals in the β Pictoris Debris Disk, *Astrophys. J.* 798, 83-100 (2015).
10. Beust, H., & Morbidelli, A., Falling Evaporating Bodies as a Clue to Outline the Structure of the β Pictoris Young Planetary System, *Icarus* 143, 170-188 (2000).
11. Telesco, C. M., *et al.*, Mid-infrared images of β Pictoris and the possible role of planetesimal collisions in the central disk, *Nature* 433, 133-136 (2005).
12. Okamoto, Y. K., *et al.*, An early extrasolar planetary system revealed by planetesimal belts in β Pictoris, *Nature* 431, 660-662 (2004).
13. Wahhaj, Z., *et al.*, The Inner Rings of β Pictoris, *Astrophys. J.* 584, L27-L32 (2003).
14. Lagage, P.O. & Pantin, E., Dust depletion in the inner disk of β Pictoris as a possible indicator of planets, *Nature* 369, 628-630 (1994).
15. Lagrange, A.-M., *et al.*, Full exploration of the Giant Planet population around β Pictoris, *Astron. Astrophys.* 612, 108-112 (2018).
16. A.-M. Lagrange, *et al.*, Constraints on planets around β Pic with Harps radial velocity data, *Astron. Astrophys.* 542, A18-A23 (2012).
17. Bonnefoy, M., *et al.*, Physical and orbital properties of β Pictoris b, *Astron. Astrophys.* 567, L9-L14 (2014).
18. Koen, C., δ Scuti pulsations in β Pictoris, *Mon. Not. R. Astron. Soc.* 341, 1385-1387 (2003).
19. Koen, C., *et al.*, Pulsations in β Pictoris, *Mon. Not. R. Astron. Soc.* 344, 1250-1256 (2003).

20. Mekarnia, D., *et al.*, The δ Scuti pulsations of β Pictoris as observed by ASTEP from Antarctica, *Astron. Astrophys.* 608, L6-L10 (2017).
21. Crifo, F., Vidal-Madjar, A., Lallement, R., Ferlet, R., and Gerbaldi, M., β Pictoris revisited by Hipparcos. Star properties. *Astron. Astrophys.* 320, L29-L32 (1997).
22. Lagrange, A.-M., *et al.*, β Pictoris b post conjunction detection with VLT/SPHERE, *Astron. Astrophys.*, 621, L8-L14 (2019).
23. Snellen, I.A.G., and Brown, A.G.A., The mass of the young planet β Pictoris b through the astrometric motion of its host star, *Nature Astronomy* 2, 883-886 (2018).
24. Dupuy, T., Brandt, T. D., Kratter, K. M.; Bowler, B.P. A Model-independent Mass and Moderate Eccentricity for β Pic b, *Astrophys. J.* 871, L4-L9 (2019).
25. Marois, C., *et al.*, Direct Imaging of Multiple Planets Orbiting the Star HR 8799, *Science* 322, 1348-1352 (2008).
26. Marois, C., Zuckerman, B., Konopacky, Q. M., Macintosh, B., & Barman, T., Images of a fourth planet orbiting HR 8799, *Nature* 468, 1080-1083 (2010).
27. Kennedy, G.M. & Kenyon, S.J., Planet Formation around Stars of Various Masses: The Snow Line and the Frequency of Giant Planets, *Astrophys. J.* 673, 502-512 (2008).
28. Lagrange, A.-M., *et al.*, The position of β Pictoris b position relative to the debris disk, *Astron. Astrophys.* 546, 38-51 (2012).
29. Fortney, J. J., Marley, M. S., Saumon, D., & Lodders, K., Synthetic Spectra and Colors of Young Giant Planet Atmospheres: Effects of Initial Conditions and Atmospheric Metallicity, *Astrophys. J.* 683, 1104-1116 (2008).

Supplementary information is available in the online version of the paper.

Acknowledgments: this work has been supported by grants from the Agence Nationale de la Recherche (ANR-14-CE33-0018) and the French Labex OSUG@2020 (Investissements d'avenir – ANR10 LABX56). A.Z. was supported by CONICYT grant n. 2117053. A.M.L. thanks Florence Forbes, K. Zwincks, A. Lecavelier, J. Pepper, P. Kervella, J.C.B. Papaloizou for discussions. T.G., D.M., L.A. and F.X.S. acknowledge support from Idex UCA^{JEDI} (ANR-15-IDEX-01) and IPEV.

Author contributions: A.M.L. led the monitoring of the variations, the data reduction, analysis and interpretation of the data, and the paper writing. N. M., P. R., M.K., and F.G. participated to the data fitting and analysis. E.C., E.M., L.B. and F.X.S. brought their expertise in stellar variability. H. Beust provided analysis of dynamical stability of the system. T.G., D.M. and L.A. brought expertise on β Pictoris photometric variability. P. A.W. and F.K. brought expertise on β Pictoris spectroscopic variability. MB., S.B., A.G., J.L-B, B.P., D.P.I., L.R., A.P.S. participated to the observations.

Author Information

Correspondence and requests for materials should be addressed to anne-marie.la-grange@univ-grenoble-alpes.fr

The authors declare that they do not have any competing financial interests.

Reprints and permissions information is available at www.nature.com/reprints

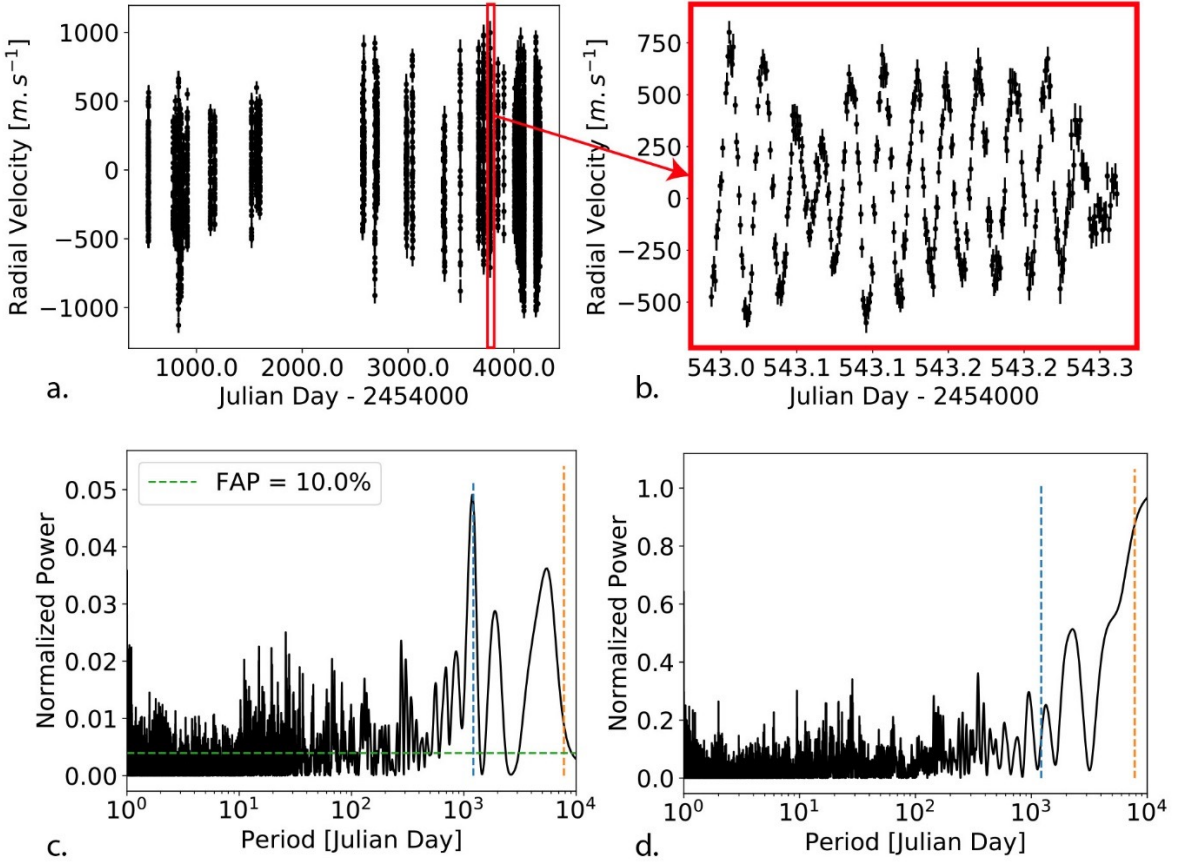


Fig. 1: RV variations of β Pic and Generalised Lomb-Scargle (GLS) periodograms. a) RV between 2008 and 2018, computed as described in Methods. The measured RV and the associated uncertainties are listed in Supplementary Table 1. The uncertainties vary depending on the SN with an average of 59 m/s and a rms of 12 m/s. b) A sequence of 6 hours of observations of β Pic obtained in January 2017. The complex, high frequency RV variations are due to stellar pulsations. c) GLS of the RV between 2008 and 2018. The 10% false alarm probability (FAP) is indicated with a horizontal line. Note that because of the pulsations and of the complex window function, peaks above the FAP do not necessarily indicate the presence of a real periodic signal at the peak position (see text). The orbital period of β Pictoris b, 7802 d, is indicated by a vertical blue dashed line. d) Zoomed-in GLS of the same dataset as in b), showing the peak above the FAP line.

cated as an orange vertical line, and that of β Pictoris c by a blue one. d) GLS of the temporal window showing the absence of a peak due to the observation window around 1200 d.

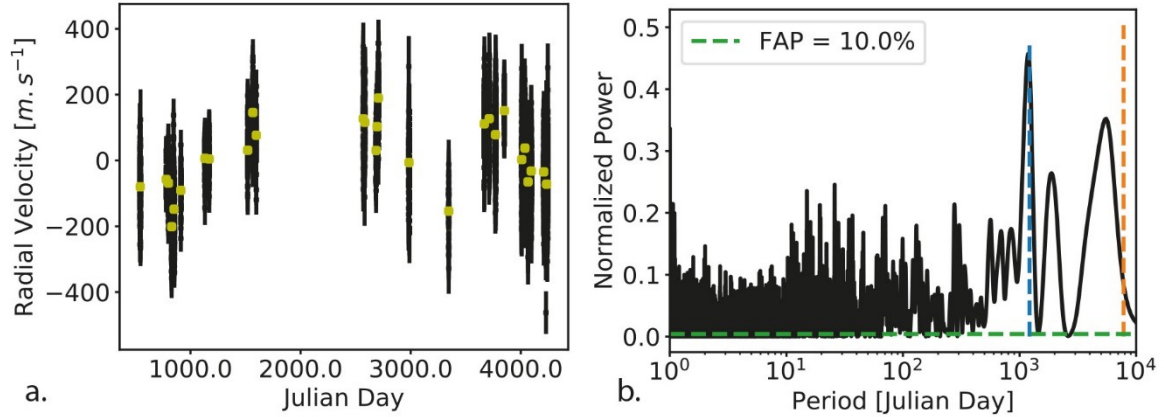


Fig. 2: Pulsations-corrected RV data with corresponding Generalized Lomb-Scargle periodogram. a) Pulsations-corrected RV data. b) Corresponding Generalized Lomb-Scargle periodogram. False alarm probability of 10% is indicated. The orange dashed, vertical line indicates the period of β Pictoris b, and the blue one the period of β Pictoris c.

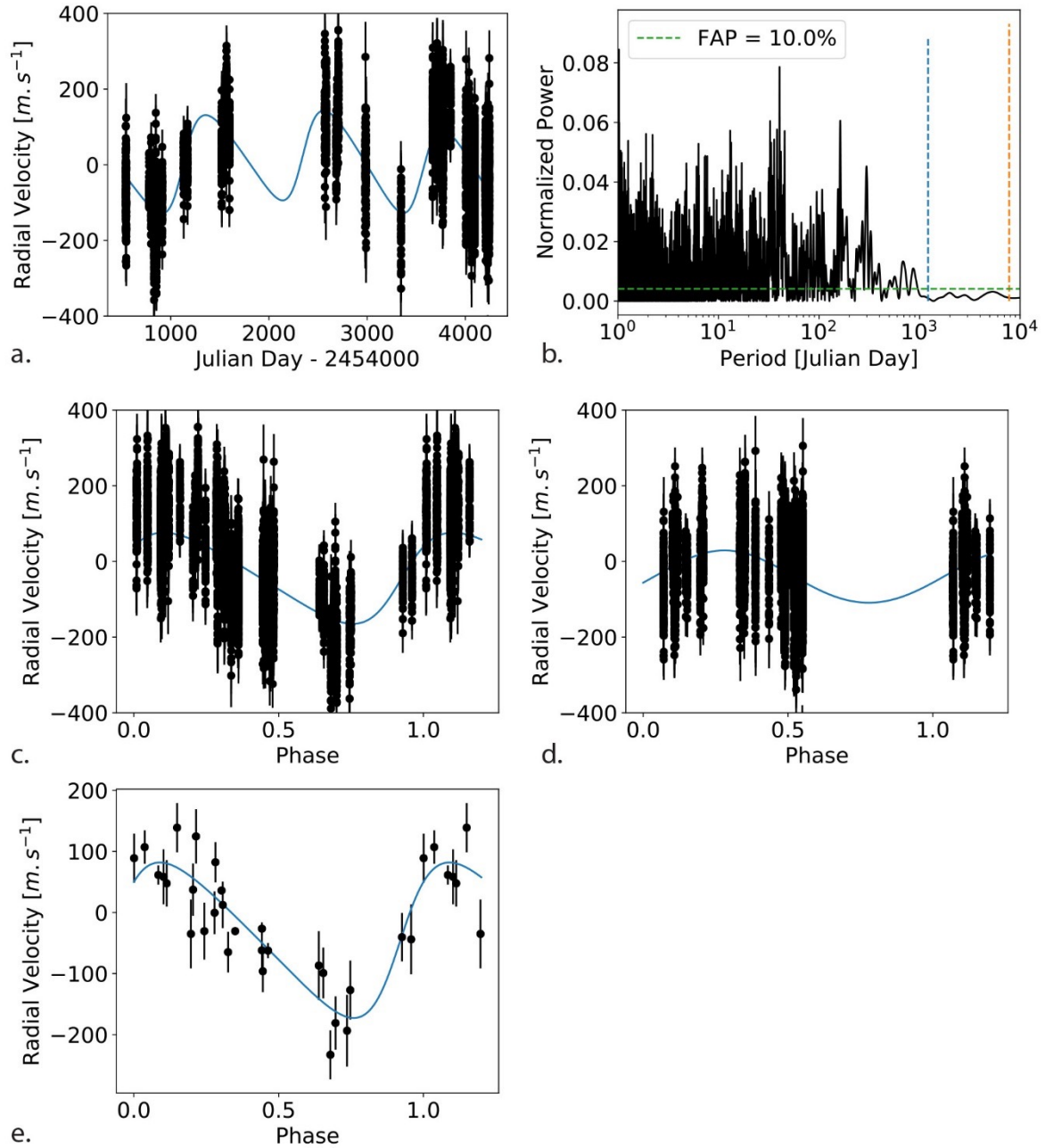


Fig. 3: Keplerian fits of the pulsation-corrected RV data. a) 2-Keplerian fit of the pulsations-corrected RV using as an input the best orbital solution of the fit of β Pictoris b astrometry (#108). b) Generalized Lomb-Scargle periodogram of the residuals after removing both planets signals. c) Pulsations-corrected and β Pictoris b-corrected RV, phased to β Pictoris c period; the β Pictoris c orbital solution is shown as a solid blue curve. d) Pulsations-corrected and β Pictoris c-corrected RV, phased to β Pictoris b period; the β Pictoris b orbital solution is shown as a solid blue curve. Note that be-

cause of the limited time baseline, β Pictoris b phases are not fully covered. e) β Pictoris b-corrected offsets, phased at β Pictoris c period. The orbital solution found for β Pictoris c is shown as the blue curve. Note that the mass of β Pictoris b was fixed to that found in the Keplerian fit shown in a, c, and d, because there are not enough data points to allow this mass to be a free parameter.

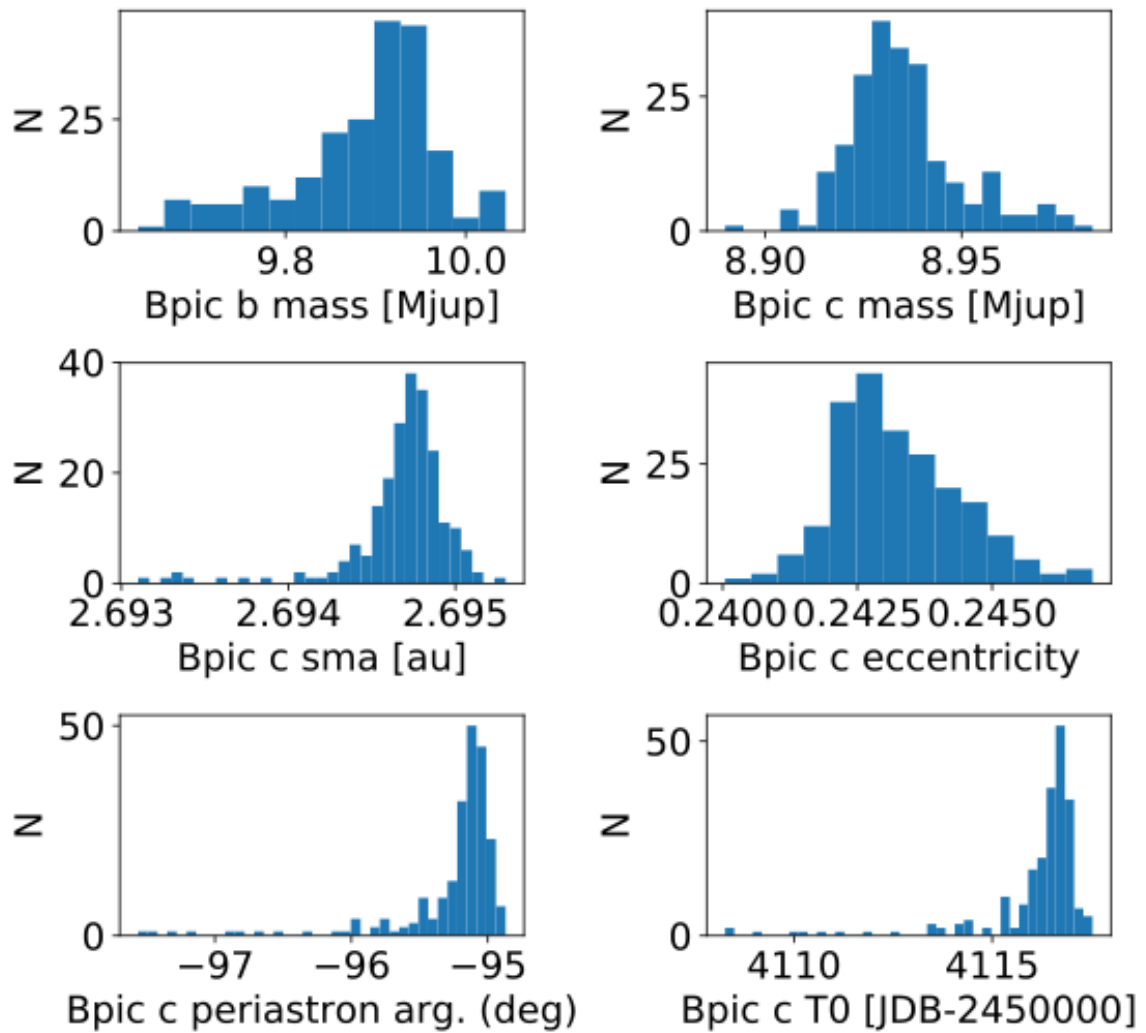


Fig 4: Histograms of the semi major axis (au), eccentricity, periastron argument ($^\circ$) and periastron time (JDB-2454000), of β Pictoris c and the masses of the two planets (M_{Jup}).

Methods

1. Data and RV measurements

A total of 6035 high resolution spectra of β Pic were obtained between October 2003 and April 2018. We removed the data taken with air mass larger than 2.0 to avoid any potential shift due to a poor centring of the star on the fibre. We also removed the few data with the lowest SN and highest SN (to avoid possible saturation effects) in order to keep the SN at 550 nm in the range 120-500. As explained in the main text, we started in March 2008 to record continuous, typically 1.5-2 hr sequences of spectra; only these spectra were selected for the present analysis.

To compute the RV and associated uncertainties, we used the SAFIR code³⁰, which was developed to measure accurate RV of rapidly rotating stars such as β Pic, and associated uncertainties that include the photon noise and the instrumental uncertainties. Basically, the code consists in correlating in the Fourier space, each spectrum of the star and a reference spectrum that is built by averaging all the available spectra of the star. The RV computed by SAFIR are then relative to this reference spectrum.

To correct for possible global chromatic effects (e.g. due to atmospheric absorption, seeing, atmospheric refraction residuals), we implemented in SAFIR the possibility to normalise each spectrum (before computing the RV), in order to obtain the same evolution of the average flux at the center of order as a function of the order, based on the reference spectrum. This normalisation does not change the measured RV within the uncertainties. Second, as variations of the local continuum within the orders directly impact the RV, particularly in the case of highly rotating stars such as β Pic (however moderated by filtering low spatial frequencies), and as there may be

variations to a few % level (e.g. due to blazes plus calibration lamp residuals³¹), we also normalised the continuum of each spectrum locally (within each order) to that of the reference spectrum, before computing the RV. This local normalisation allows correcting the continuum from potential variations occurring *within* the orders. We obtained thus two RV time-series (with and without this local normalisation). The two corresponding time series appear to be comparable within uncertainties except on JDB= 2456773. As this indicates a significant and uncontrolled change in the blaze, we did not take these specific data into account in the rest of the study. The RV obtained after averaging the two time series are shown in Fig.1 and listed in Extended Data Table 1.

Note: A major instrumental change was made in HARPS in 2015, that included the installation of a new set of fibres and scrambling capabilities. To our knowledge, the impact of this change was estimated only in the case of low rotating stars³². To check the impact of this change, we computed first the RV of the data obtained before and after this change separately (using thus two references), and then the RV using all the data (using here one reference only). No change was detected within the uncertainties. This means that the impact is smaller than 10-20 m/s.

2 Correction from stellar pulsations

The measured RV were used to compute the Generalized Lomb Scargle periodogram and identify a peak at 1180 ± 130 d, as described in the Main text.

As a second step, we corrected the RV from the high frequency pulsation pattern. To do so, we used long enough (1.5-2 hr or more) continuous sequences, presenting at least 3-4 well sampled extrema, in order to estimate as accurately as possible the pulsation pattern. Sequences not complying with this criterion were then removed. In rare cases, the sequences were (slightly) shorter but repeated during the same night

or repeated over consecutive nights or nights separated by less than 8 nights; these sequences were kept. Finally, data separated by less than 8 d were gathered in groups. A total of 28 groups (with 5108 data points) were selected according to the afore mentioned criteria. The corresponding RV are shown in Figure 2 in a single figure and detailed in Extended data Figure 1.

To correct for the stellar pulsations, we used 3 different approaches and several methods within these. The first approach (method 1 below) consists in averaging the data considered for each group. A second approach (methods 2 to 4 below) consists in fitting the pulsations by sine functions and an offset in an iterative way. Lastly, our third approach (method 5) consists in fitting the data simultaneously by sine functions plus an offset. The various methods are described below.

- Method 1: An average of the RVs was computed for each group of data. This method is accurate only when several pulsations are monitored and are properly (regularly enough) sampled. This is not the case at JDB= 2454780, 2457344, 2457849, and to a lower extent, 2455170, 2456579 and 2456583 (See Extended data Figure 1).
- Method 2: Each data group was independently fitted with a sine function (3 free parameters), plus a zero-point offset. The zero-point offset is justified by the fact that long-term (> 1000 d) variations are present, and that the RV are relative to the RV of a reference spectrum. 1000 fits were made with frequencies guesses between 0.014 and 0.034 d^{-1} and the best fit was kept. The corresponding sine function was then subtracted. We repeated this fitting process 9 times. Hence, each group was fitted by 10 sine functions plus an offset, which corresponds to a total of 31 free parameters. In most cases, the offset and the rms of the residuals converged rapidly, after few (typically 3) iterations. In a few cases, the offset has not

fully stabilised at the 10th iteration, but the residuals were much lower than the uncertainties (computed below). The 5 data groups corresponding to the longest sequences and a large number of data points, were fitted with 30 sine functions instead of 10, assuming that the length of the sequence allows to characterise more pulsations, to be possibly compared with the 31 pulsations derived from the photometric analysis of Mekarnia et al²⁴. The convergence was reached within typically 15 iterations. The fits of the pulsations are shown in Extended Data Figure 1 for each group, and the offset values and associated uncertainties (see below) are listed in Table S.2. The number of nights in each data group, the number of points and the rms of the RV residuals after subtraction of the fitted pulsations and offset are also given in this table. To compute the uncertainties associated to the offsets, we proceeded as follows: for each group, we generated a synthetic RV time series using the 30 pulsation frequencies found in the fit of the Jan. 2017 data (755 points) with the time sampling associated to this group. We assumed that this provides a realistic representation of the pulsations observed both at high frequency (in the δ Scuti domain) and in the low frequency (1–10 d⁻¹). For each point of the data group, we added Gaussian random noise to the synthetic RV time series, with a rms equal to the RV uncertainties for this point. We then fitted each synthetic RV time series using the same step-by-step procedure as described above. The expected offsets for each of these fits should be zero. This process was repeated 1000 times, after shifting the temporal sequence in order to probe different positions in the time series (nodes, noise realisations, etc). The rms of the 1000 values of the offsets provides an uncertainty associated with the time sampling and therefore with the RV of the corresponding data group. The median (resp. rms) of the resulting uncertainties is 31 (resp. 11) m/s. We then added, for each group, an un-

certainty equal to half the difference between the offsets measured with the SAFIR usual method and the additional local normalisation described above.

- Method 3a: we fitted a long sequence obtained in Jan. 2017 (7 nights, 755 points, including a long continuous 6.5 hours sequence) as in Approach 2. We then applied the same iterative method as in Method 2 to each of the 27 other data groups, while keeping the periods equal to those found in the fitting of the Jan. 2017 data. We assumed then here that the *frequencies* of the pulsations do not vary over our time basis (between 2008 and 2018). The phases were free because our precision on the periods is not enough to fix them, and the amplitudes were also free, to account for possible temporal variations.
- Method 3b: same as 3a/ but using the periods obtained in the fit of the October 2017 data (508 points).
- Method 3c: same as 3a/ but using the periods obtained in the fit of the Spring 2017 data (782 points).
- Method 4: same as 3a/ but using the first 13 periods given by the photometric analysis of Mekarnia et al²⁴.
- Method 5: each data group was fitted simultaneously by 10 sine functions plus an offset. To do so, an evolutionary algorithm was used. To estimate the uncertainties associated to the offsets, 100 time series were generated where each RV data point was replaced by a random value drawn according to a Gaussian law centered on the original RV with a sigma equal the uncertainty of the measurement $N(RV, uncertainty)$. These time series were fitted, and a new series was created with, for each date, the average of the resulting offsets, and with the rms of the offsets as uncertainties.

Extended Data Figure 2 shows the offsets obtained with these different methods, and Table S.2 lists the offsets obtained with Method 2 and their associated uncertainties. As expected, the differences are larger when comparing Method 1 and Methods 2-5 when the sequences are short and/or not well sampled (see above). The rms of the differences between the offsets obtained with Methods 1 and 2 is 20 m/s when considering all epochs and is reduced to 10.6 m/s if we do not consider the poorly sampled datasets obtained in JDB-2450000 = 4780, 7344, 7849. It is further reduced to 8.2 m/s when we do not consider in addition JDB-2450000 = 5170, 6569, and 6583. The offsets obtained with Methods 2-5 are in excellent agreement, with averaged differences between Methods 2 and 3a (resp., 2 and 3b, 2 and 3c, 2 and 4, 2 and 5) of less than 2 m/s and rms of 6.5 (resp. 8.1, 8.5, 8.8 and 8.2) m/s.

Noticeably, most of the high amplitude pulsations found in Method 2 are in agreement with the analysis of the photometric data²⁴. In the long sequences, at least 7-8 frequencies found in the RV fit are also found by Mekarnia et al²⁴ analysis of photometric data. The fact that Methods 2 and 4 give very similar results indicate that the fit of the lowest amplitudes pulsations does not impact the offsets and the long-term variations of the residuals.

The fits of the longest groups moreover reveal additional, low frequency (2-6 cycles.d⁻¹) pulsation(s) with an amplitude of about 40 m/s, i.e. 6 to 11 times lower than the main pulsation peak. Main Sequence A-F stars showing pulsations with periods in the range 0.25-3 days are classified as γ Dor pulsators and the pulsations are attributed to high-order g-modes. We conclude that β Pic might belong to the small group of "hybrid" δ Scuti/ γ Dor stars, mostly detected using long and continuous monitoring by Corot and Kepler³⁵. Finally, some low amplitude variations on times scales of 10-30 days could be present as well, as seen in the longest sequences, but

the available data do not allow to characterise them. Yet, we checked that such pulsations do not create high peaks at longer periods, even considering beats between several pulsations.

3. Could the RV residuals be spurious?

The 1000 simulated time series described in Methods, Section 2, to estimate the uncertainties were used to check whether the pulsations can produce long term RV variations similar to those observed. We computed the periodogram for each time series, and the maximum power in the range 1100-1300 day range. The maximum power (at the 1% level) is slightly below the FAP and is far below the peak amplitude of the 1200 d peak observed in the periodogram of the raw RV time series or that of the pulsations corrected RV ones. Also, the periodogram of the RV time series with offsets subtracted does not show a peak above the FAP. Hence, the pulsations do not lead to a significant peak at 1200 d.

4. Dynamical impact of an additional planet

4.1 Stability of the 2-planet system

The ratio of β Pic b and β Pic c semi-major axis is about 3.5, so the system is presumably stable. Supplementary Data Figure 4 shows an example of secular evolution of the semi-major axis and eccentricity of the two planets over 1 Myr, as computed with the symplectic code HJS³⁴. The real computation was extended up to 50 Myr and does not reveal any change with respect to the 1 Myr case. We note that the semi-major axes are extremely stable, while the eccentricities exhibit moderate regular fluctuations. This is characteristic for regular dynamics and allows us to conclude that the system is stable. Interestingly, we note that β Pic b's eccentricity secu-

larly oscillates between ~ 0 and 0.15. This shows that β Pic c is able to excite β Pic b's eccentricity. Conversely, the eccentricity of β Pic c never reaches zero. This means that at least part of the planet eccentricity cannot be explained by the sole perturbing action of β Pic b and must be primordial.

4.2 Impact on the FEB scenario

Dynamical studies, based on the large number of observed FEB events have shown that the presumed star-grazing asteroids or comets probably originate from internal mean-motion resonances (4:1 or 3:1) with a Jovian planet orbiting β Pic at ~ 10 au with moderate eccentric orbit ($e \sim 0.1$)^{35,36}. β Pic b was then identified as the planet responsible for the FEB phenomenon, even though its mass ($\sim 9 M_{\text{Jup}}$) is larger than the one estimated originally ($\sim 2 M_{\text{Jup}}$). To explain the velocity distribution of the observed blueshifted and redshifted absorptions, an additional, less massive, possibly terrestrial-mass planet orbiting more or less at the current location of β Pic c³⁵ was proposed. The secular evolution of the semi-major axis and eccentricity of the two planets over a period of 1 Myr, computed with the symplectic code HJS³⁴, yields variations of the sma and eccentricity of β Pic b of about 0.015 au and of eccentricity 0.1 respectively, and less than 5e-3 au and less than 0.15 for β pic c. Note that the two separate families of FEBs were confirmed recently⁵ based on a larger set of data. In this scenario, the masses of the planets are much smaller than the masses of the observed planets. Thus, new simulations are needed to see whether the FEBs can be generated under these new conditions. In fact, the presence of β Pic c might actually enhance the FEB generation process. As seen above, β Pic c is able to secularly excite β Pic b eccentricity to larger values than previously considered, leading to more efficient resonances and enhancement of the FEB generation process. Indeed, with a larger eccentricity, other mean-motion resonances like 5:2 may become

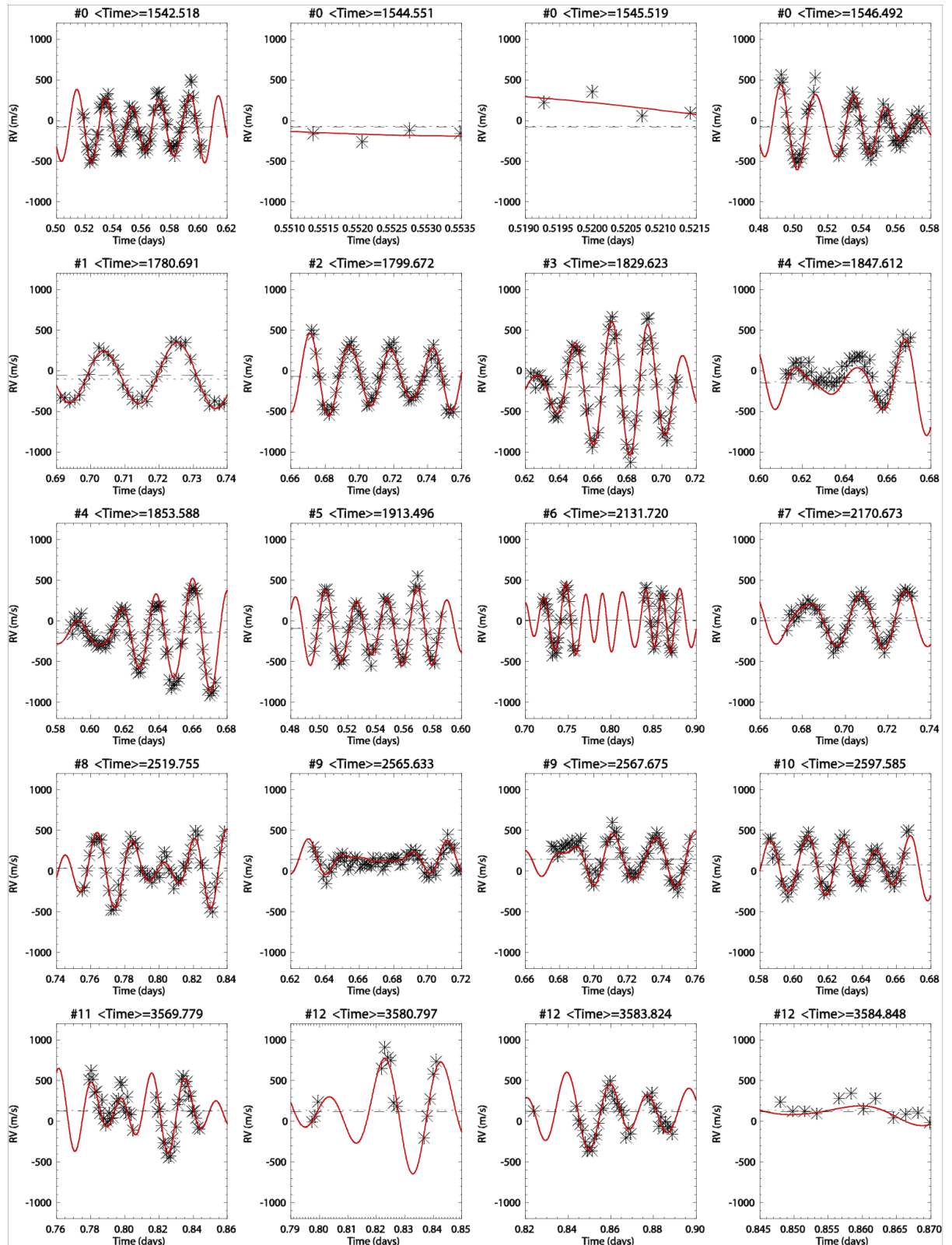
additional sources of FEBs that were not considered before. β Pic c itself is able, to a moderate extent, to excite the eccentricities of FEB progenitors locked in mean-motion resonances with β Pic b and contributing to the FEBs. Of course, the number of progenitors that will actually become FEBs despite encounters with β Pic c, is a key issue. The high mass of β Pic b might create resonances ranges wider than previously. Also, with a higher mass, the resonant eccentricity increase that drives progenitor to the FEB state is faster. Various aspects of this scenario will be the purpose of future work.

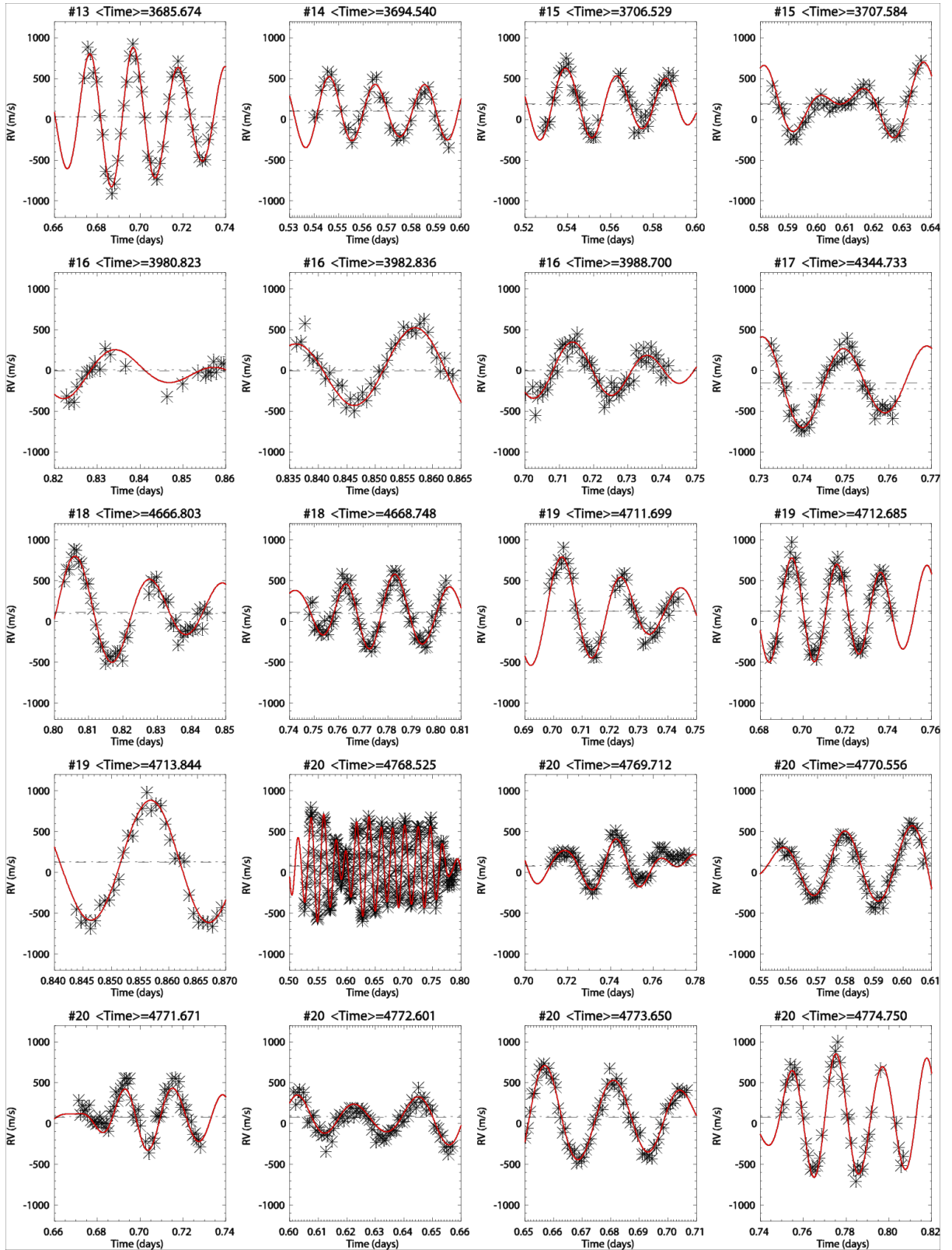
Data availability: the HARPS spectra are available in the ESO archive, and the measured RV data are given in Table 1 of the Supplementary Information.

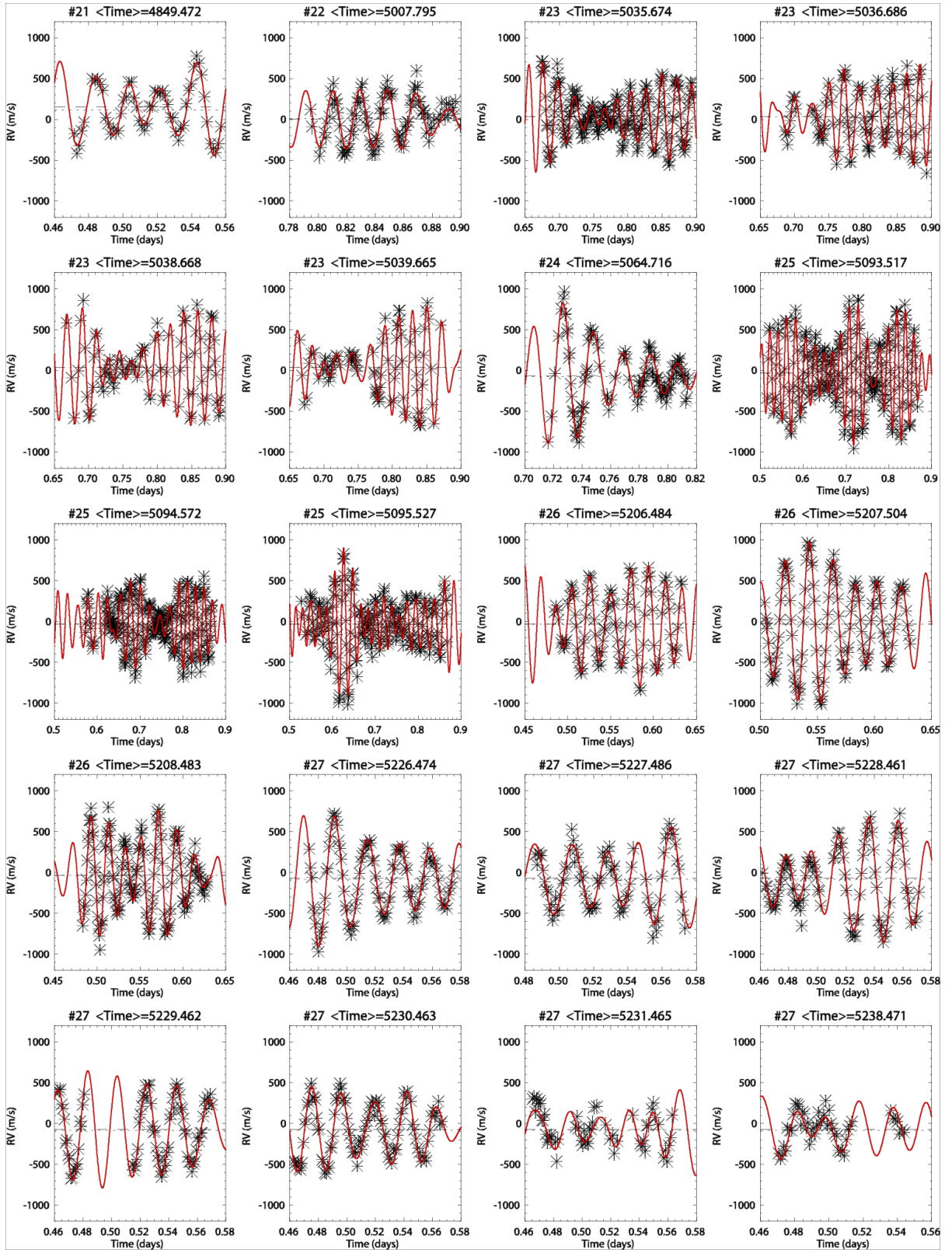
Code availability: the codes used for this paper are home-made codes

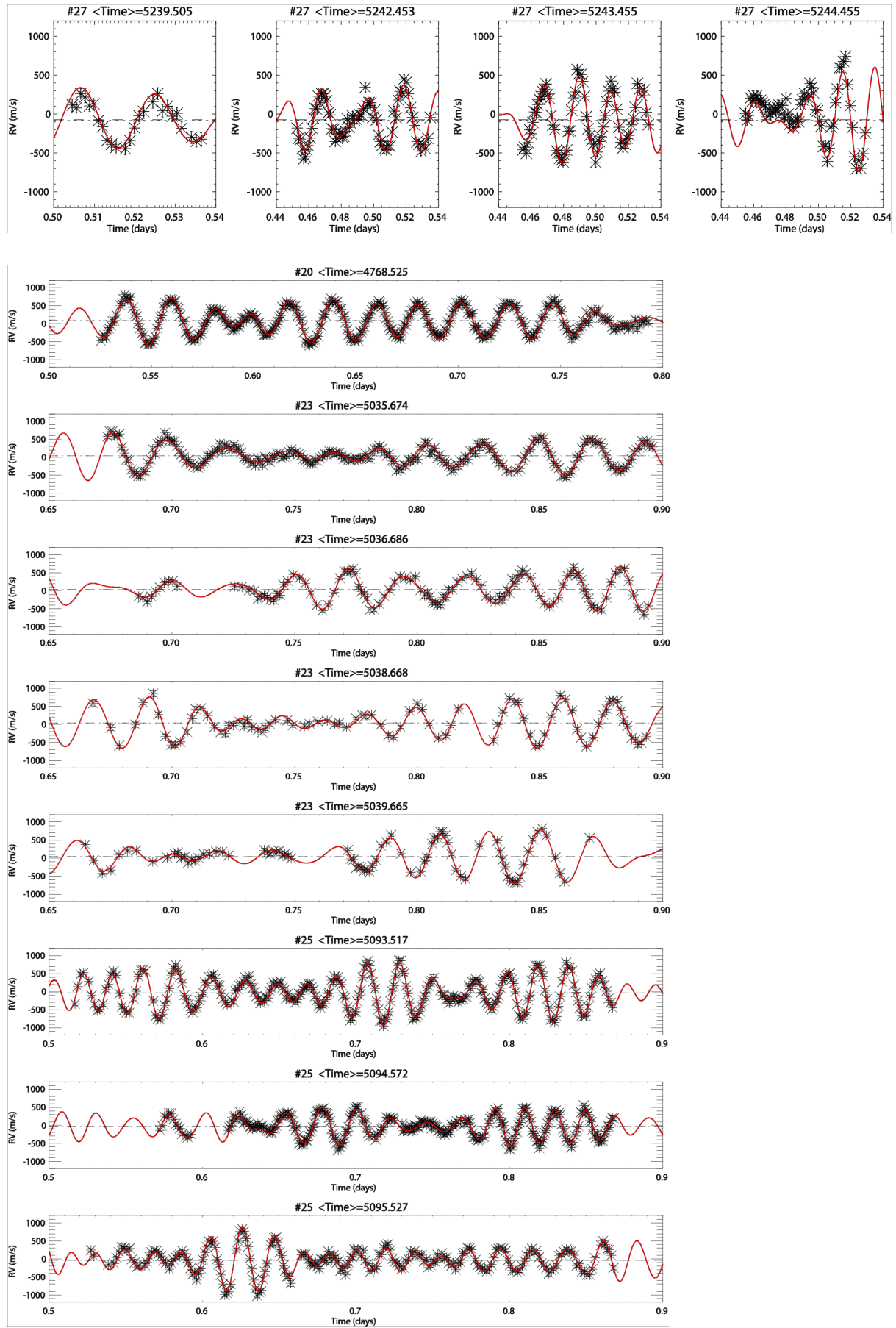
30. Galland F., *et al.*, Extrasolar planets and brown dwarfs around A-F type stars. I. Performances of radial velocity measurements, first analyses of variations, *Astron. Astrophys.* 443, 337-345 (2005).
31. Anglada-Escudé, G., & Butler, P. R., The HARPS-TERRA Project. I. Description of the Algorithms, Performance, and New Measurements on a Few Remarkable Stars Observed by HARPS, *Astrophys. J. Suppl.* 200, 15-34 (2012).
32. Lo-curto, G., *et al*, HARPS Gets New Fibres After 12 Years of Operation, *Messenger* 162, 91-15 (2015).
33. Bradley, P.A., *et al*, Analysis of γ Doradus and δ Scuti stars observed by Kepler, *Astronomical journal* 149, 68-81 (2015)
34. Beust, H., Symplectic integration of hierarchical stellar systems, *Astron. Astrophys.* 400, 1129-1144 (2003).

35. Beust, H. & Morbidelli A., Mean-Motion Resonances as a Source for Infalling Comets toward β Pictoris, *Icarus* 120, 358-370 (1996).
36. Thebault, P. & Beust, H., Falling evaporating bodies in the β Pictoris system. Resonance refilling and long term duration of the phenomenon, *Astron. Astrophys.* 376, 621-640 (2001)

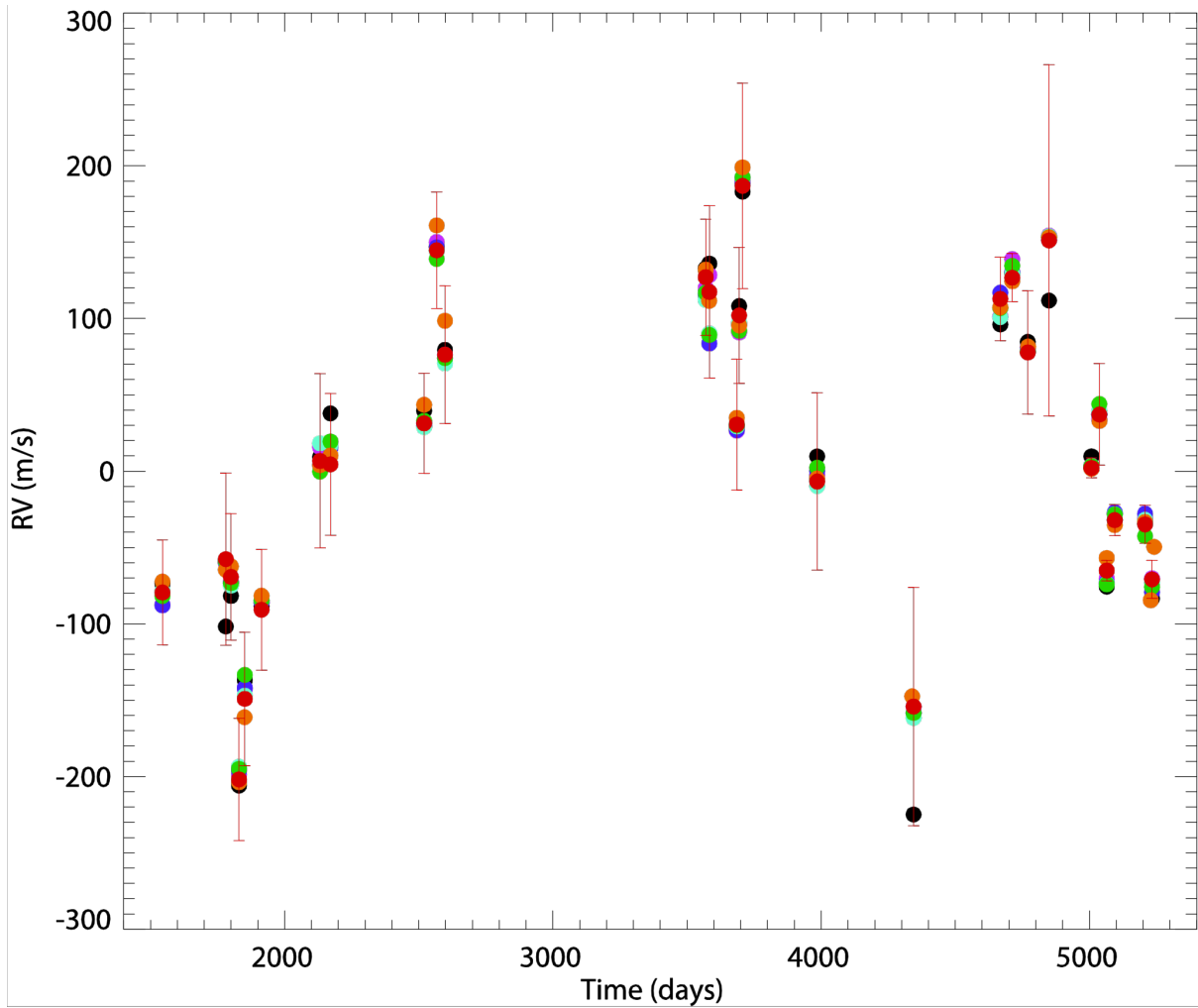




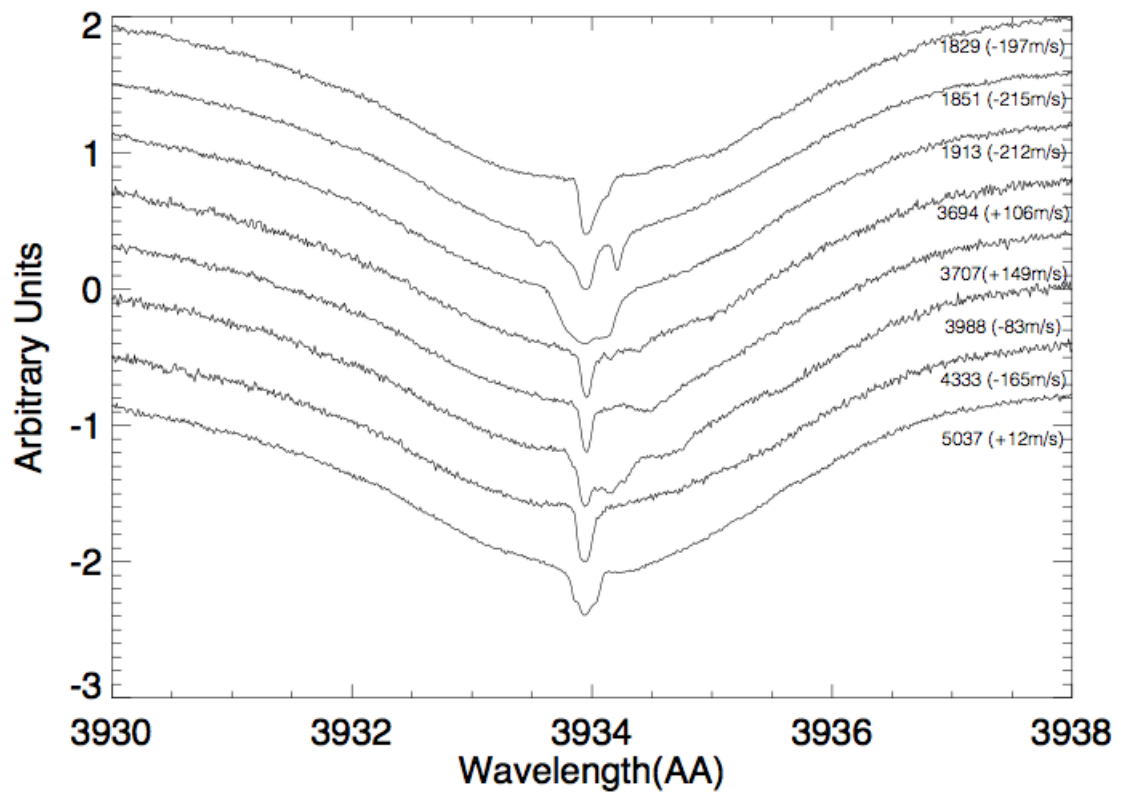




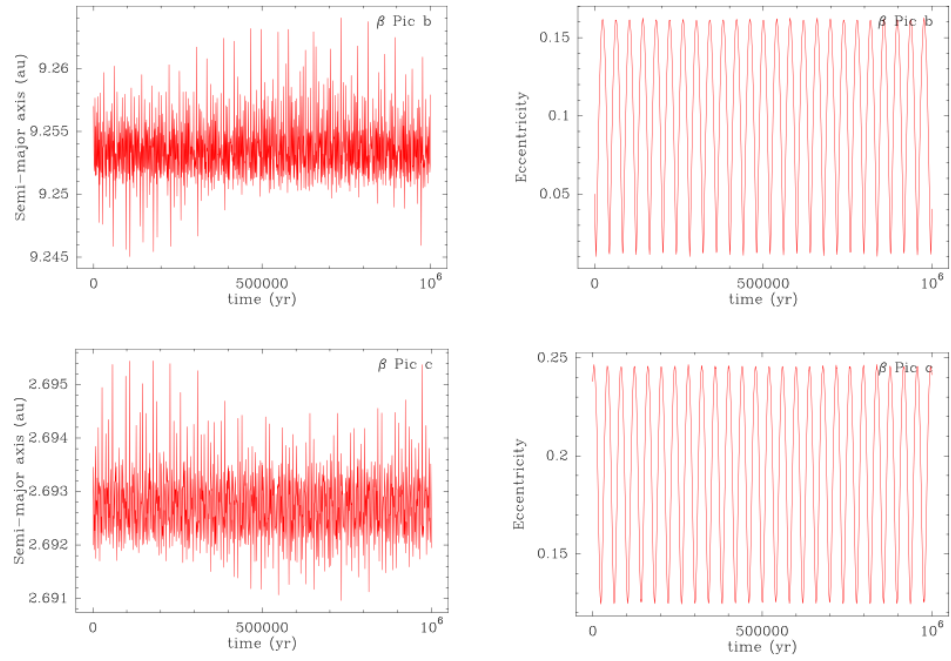
Supplementary Figure 1: Observed RV sequences and uncertainties (black) versus time (Julian Days – 2453000, where <time> is indicated on the top of each figure). The fits from approach 2 are indicated (red). Note that sequences with the same number belong to the same group and are fitted together. All nights are shown. Finally, zooms on the nights of long durations are provided.



Supplementary Figure 2: Offsets obtained with different methods as a function of time (Julian Days-2453000), as described in Methods 2., before removal of the β Pic b signal. Method 1 (average, black). Method 2 (step-by-step fits with periods as free parameters and uncertainties from Methods 2., red). Method 3a (step-by-step fit with fixed periods derived from the fit of January data, pink). Method 3b (step-by-step fit with fixed periods derived from the fit of October 2017 data, purple). Method 3c (step-by-step fit with fixed periods derived from the fit of October 2017 data, bright blue). Method 4 (step-by-step fit with 13 fixed periods from the photometric observations²², green). Method 5 (direct fits with free periods, orange).



Supplementary Figure 3: Examples of FEBs as seen in the Ca II K line. The JDB-2453000 dates are indicated close to the spectrum. In parenthesis is given the offset of the RV at the same epoch.



Supplementary Figure 4: example of secular evolution of the two planets (semi-major axis and eccentricity) over 1 Myr as computed with the symplectic code HJS³⁹.

Supplementary Data Table 1: RV data (see attached)

Supplementary Data Table 2: time (in Julian Days-2453000), RV offsets from approach 2, associated uncertainties, number of nights in the group, number of points and rms of the RV residuals.

JDB-2453000	RV(m/s)	σ RV (m/s)	nNG	Np	rms	RVres
1544.402222	-79.5	34.4	4	164	74.3	
1780.715088	-57.6	56.4	1	35	38.6	
1799.713379	-69.3	41.5	1	65	58.6	
1829.666260	-201.9	40.1	1	72	70.4	
1851.327148	-149.2	43.6	2	130	96.7	
1913.540771	-90.8	48.2	1	61	56.2	
2131.798584	6.7	39.6	1	54	49.9	
2170.702148	4.4	57.1	1	55	47.4	
2519.796387	31.3	46.5	1	60	67.0	
2566.704102	144.6	32.9	2	131	64.2	
2597.626953	76.3	38.1	1	66	59.8	
3569.811523	127.0	45.0	1	50	94.7	
3583.385498	117.4	38.0	3	64	79.8	
3685.703369	30.5	56.4	1	43	61.7	
3694.567627	102.0	42.9	1	40	67.1	
3707.084717	186.8	44.6	2	100	75.0	
3985.245850	-6.8	36.1	3	118	88.9	
4344.747070	-154.2	58.6	1	50	74.1	
4668.008301	112.8	40.1	2	132	74.3	
4712.636719	126.7	27.4	3	151	78.6	
4770.451172	77.7	15.7	7	755	72.5	

4849.514648	151.1	40.4	1	55	55.1
5007.846191	2.1	35.0	1	98	107.2
5037.192383	37.1	6.6	4	508	68.7
5064.770508	-65.1	33.3	1	106	85.5
5094.640137	-32.1	6.7	3	766	69.1
5207.680664	-34.9	10.2	3	390	65.1
5233.605957	-70.9	12.4	7	789	84.5

Supplementary Data Table 3: Mass and orbital parameters of β Pictoris c and mass of β Pictoris b obtained by fitting either the pulsations corrected RV or the offsets computed while fitting the pulsations. Column 2 : average of the parameters obtained from 219 fits of the 5108 RV residuals once corrected from the pulsations using Method 2, using 219 orbital solutions for β Pictoris b (see text). Column 3: same as Column 2, but fitting the 28 offsets deduced from Method 2 instead of the 5108 data points. Column 4: Parameters found fitting the 5108 data points once corrected from the pulsations using Method 2, using the best orbital solutions for β Pictoris b (see text). Column 5: same as Column 4, but fitting the 28 offsets deduced from Method 2 instead of the 5108 data points. Column 6: same as Column 2, but Method 5 was used instead of Method 2 to compute the residuals. Column 7: same as Column 4, but Method 5 was used instead of Method 2 to compute the residuals. The uncertainties in Columns 4 and 5 were computed as described in the text. The uncertainties in Columns 2 are the sum of the uncertainties of Column 4 and the uncertainties measured in the histograms shown in Figure 4. Same principle for the uncertainties in Columns 3, 6 and 7. It can be seen that 1/ the results obtained using Methods 2 and 5 are in excellent agreement, 2/ the uncertainties associated to the orbital parameters of β Pictoris b have a negligible impact on the masses and on the orbital parameters of β Pictoris c, and 3/ the results obtained using the 5108 data points and the offsets are also in agreement, but using the offsets lead to larger uncertainties.

	Pulsation corrected RV -all suitable RV points method 2	Pulsation corrected RV on offsets.	Pulsation corrected RV -all suitable RV points method 2	Pulsation corrected RV on offsets.	Pulsation corrected RV -all suitable RV points method 5	Pulsation corrected RV -all suitable RV points, method 5
Data points	5108	28	5108	28	5108	5108
Number of β Pictoris b orbital solutions considered	219	219	1 #108 Fig. 2	1 #108 Fig. 2	219	1 #108 Fig. 2
P[days]	1218 ± 2	1222 ± 14	1218 ± 2	1117 ± 14	1213 ± 3	1218 ± 3
T_0 [JDB-2450000]	4116 ± 9	4116 ± 316	4116 ± 9	4117 ± 316	4213 ± 13	4128 ± 13
e	0.24 ± 0.02	0.27 ± 0.02	0.24 ± 0.02	0.27 ± 0.02	0.21 ± 0.03	0.21 ± 0.03
omega [deg]	-96 ± 3	-94 ± 24	-96 ± 3	-94 ± 24	-94 ± 3	-96 ± 3
K [m/s]	113 ± 2	118 ± 12	113 ± 2	119 ± 12	117 ± 2	118 ± 2
$\sigma_{\text{go-c}}$ [m/s]	81 ± 1	45 ± 7	81 ± 1	45 ± 7	82 ± 1	82 ± 1
m_P [M_{Jup}]	8.93 ± 0.14	9.4 ± 1.2	8.95 ± 0.14	9.4 ± 12	9.16 ± 0.18	9.19 ± 0.18
a_P [au]	2.69 ± 0.003	2.70 ± 0.02	2.69 ± 0.003	2.70 ± 0.02	2.69 ± 0.004	2.69 ± 0.004
$M_{\text{BPic b}}$ (M_{Jup})	9.9 ± 0.5	(fixed to 9.9)	9.8 ± 0.5	(fixed to 9.9)	10.4 ± 0.7	10.3 ± 0.7